nature physics

LETTERS

https://doi.org/10.1038/s41567-019-0650-1

Kibble–Zurek universality in a strongly interacting Fermi superfluid

Bumsuk Ko[1,2], Jee Woo Park[1*] and Y. Shin[1,2*]

The Kibble–Zurek mechanism describes the spontaneous formation of topological defects in a system crossing a continuous phase transition[1,2]. Its central premise is the notion of universality, which states that the characteristic scaling exponent describing the dependence of the defect density on the quench rate is determined by the underlying symmetries of the system. Whether this universality can be extended to strongly interacting systems, such as a unitary Fermi gas, is an open question that has recently drawn attention in the context of holographic theories[3,4]. Here, we report the observation of the Kibble–Zurek universality in a strongly interacting Fermi superfluid. As the microscopic nature of superfluidity is tuned from Bose–Einstein condensation of tightly bound molecules to Bardeen–Cooper–Schrieffer superfluidity of long-range fermion pairs, the thermal quench formation of vortices reveals a constant scaling exponent arising from the *U*(1) gauge symmetry of the system. In rapid quenches, destructive vortex collisions lead to the saturation of vortex densities, the values of which can be universally scaled by the interaction-dependent area of the vortex cores. This work paves the way for precision studies of non-equilibrium dynamics in a highly tunable, strongly correlated many-fermion system[5,6].

Near a continuous phase transition, the characteristic length- and timescales of a system's correlation diverge, giving rise to collective phenomena that are largely decoupled from the microscopic details of the system[7]. The Kibble–Zurek (KZ) mechanism for the creation of topological defects presents a paradigmatic example of such universal dynamics[1,2]. When the temperature T of a system is cooled across the critical temperature T_c for a continuous phase transition, the diverging relaxation time τ will eventually exceed the timescale for the change in temperature, at which point the system can no longer follow the externally imposed quench. Consequently, the system's correlation length ξ becomes frozen at a value $\hat{\xi}$ until its reflexes are recovered in the broken-symmetry phase. This leads to the formation of domains of size $\hat{\xi}$ with independent order parameters, which merge to create topological defects at their boundaries.

The essential prediction of the KZ theory is the existence of a universal scaling relationship between the defect density and the quench rate. Specifically, for a linear temperature quench, the defect density will have a power-law dependence on the quench rate, with a characteristic exponent α_{KZ} determined by the critical exponents ν and z of the system. Here, ν and z describe the divergence of ξ and τ through $\xi=\xi_0|(T-T_c)/T_c|^{-\nu}$ and $\tau=\tau_0|(T-T_c)/T_c|^{-\nu z}$, where ξ_0 and τ_0 are the microscopic length- and timescales of the system, respectively. Since systems that fall into the same universality class have a shared set of critical exponents determined by generic factors such as the underlying symmetries, range of interactions and dimensionality, the KZ exponent will also be universally determined by these factors.

Unlike previous investigations of the KZ mechanism[8–18], strongly interacting atomic Fermi gases with tunable interactions offer a unique opportunity to explore the mechanism's universal aspects in a setting where the system's microscopic description can be consistently and dramatically tuned. In the vicinity of a Feshbach resonance, as the scattering length between the spin-up and spin-down fermions is tuned from positive to negative, the nature of superfluidity changes from Bose–Einstein condensation (BEC) of tightly bound molecules to Bardeen–Cooper–Schrieffer (BCS) superfluidity of long-range fermion pairs[19,20]. This leads to strong variations in the static and dynamic properties of the superfluid, as apparent in the changes of the critical temperature[21–23] and the critical velocity[24–26] in the BEC–BCS crossover. Furthermore, in the unitary regime, the diverging scattering length gives rise to a novel form of strongly correlated fermionic superfluidity with a scale-invariant nature that provides connections to other exotic states of matter such as those found in neutron stars and quark–gluon plasma[6,20,27]. Nevertheless, the spontaneous breaking of the $U(1)$ gauge symmetry associated with the normal-to-superfluid phase transition should prevail throughout the crossover, and the question of whether the KZ mechanism can be consistently applied in this regime remains largely unaddressed.

Here, we report the observation of the KZ universality in a strongly interacting Fermi superfluid. A linear temperature quench in an oblate sample of ^{6}Li atoms near a Feshbach resonance spontaneously creates as many as 50 vortices in the superfluid phase with counting statistics that reveal the characteristic power-law scaling of the KZ mechanism. As the interaction is tuned across the BEC–BCS crossover, the extracted critical exponents remain constant at a value that is consistent with the predictions of the inhomogeneous KZ mechanism for a BEC in a harmonic trap[28]. Interestingly, when the quench rate is sufficiently increased, the vortex density becomes saturated to a value that is strongly dependent on the interaction strength. This is explained in terms of the destructive collisions among vortices with opposite signs, whose effective range is governed by the interaction-dependent vortex core size of the superfluid. This mechanism reveals the microscopic scales involved in the critical dynamics of the superfluid, allowing the data obtained in different regimes of the BEC–BCS crossover to be collapsed into a single universal curve. Notably, these observations hold true at unitarity, where strong correlations make the investigations of the system's non-equilibrium dynamics particularly challenging[5,6].

The experiment starts with the creation of an equal mixture of ultracold ^{6}Li in its two lowest hyperfine states $|1\rangle$ and $|2\rangle$ near the broad *s*-wave Feshbach resonance located at 832 G (ref. [26]). The atoms are confined in a highly oblate trap that consists of a single-beam optical dipole trap (ODT) that provides tight axial confinement and a weak magnetic trap that provides radially symmetric

[1]Department of Physics and Astronomy, Institute of Applied Physics, Seoul National University, Seoul, Korea. [2]Center for Correlated Electron Systems, Institute for Basic Science, Seoul, Korea. *e-mail: jw_park@snu.ac.kr; yishin@snu.ac.kr

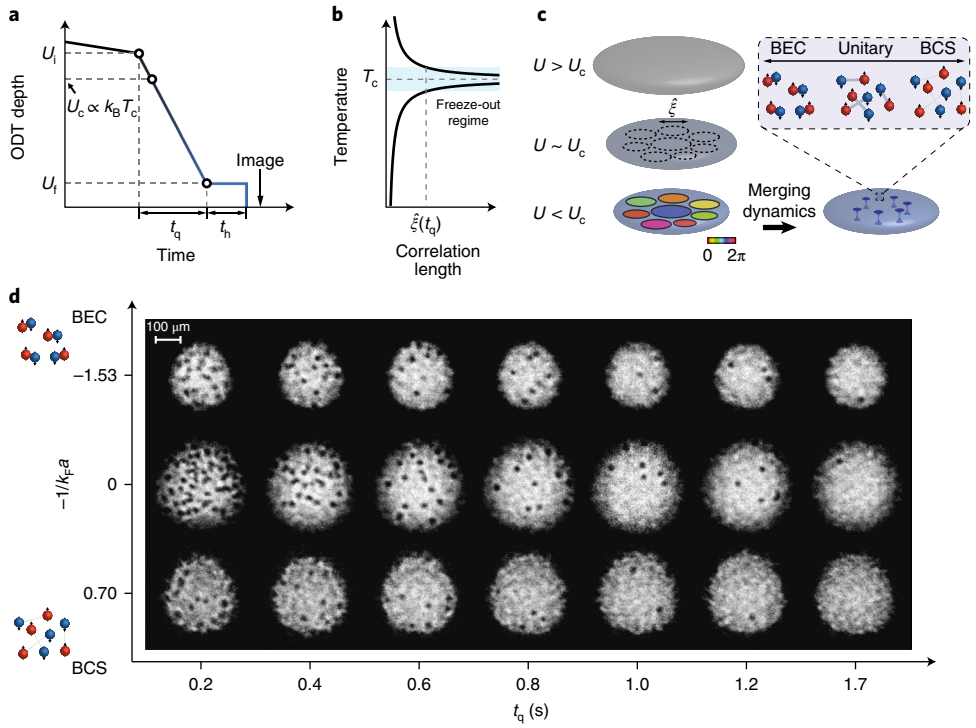

Fig. 1 | Spontaneous defect formation during the normal-to-superfluid phase transition in a strongly interacting Fermi gas. a, Schematic of the experiment. The ODT depth is initially set to $U_i = 1.15U_c$, and the gas is evaporatively cooled by linearly lowering the trap depth to U_f in a variable duration t_q. After a hold time t_h, the sample is released from the trap and an absorption image of the sample is taken. The Boltzmann constant is defined by k_B. **b**, Evolution of the correlation length and its freeze-out during the phase transition. During the quench, the critical slowing of the system's reflexes near T_c leads to the freeze-out of the diverging correlation length at $\hat{\xi}$. In the experiment, since the quench width $U_i - U_f$ is fixed, the quench time t_q determines the value of $\hat{\xi}$. **c**, Formation of quantized vortices during spontaneous symmetry breaking. On entering the broken-symmetry phase, superfluid domains with independent phases are formed, which merge to create quantized vortices at their boundaries. Patches with different colours indicate domains with different phases. Red and blue spheres with up and down arrows illustrate ^{6}Li atoms in the $|1\rangle$ and $|2\rangle$ states, respectively. The defect formation dynamics are explored across the BEC–BCS crossover. **d**, Representative images of the gas after TOF. The number of created vortices is recorded as a function of the quench duration and the interaction strength.

confinement. Initially, about 2.0×10^6 atoms per spin state are prepared at different magnetic fields around the Feshbach resonance at a temperature corresponding to 1.15 times the critical ODT depth U_c for the onset of condensation. Since the critical temperature varies across the BEC–BCS crossover as a function of the interaction strength, U_c is determined at each magnetic field accessed in the experiment (see Methods). The mixture is then evaporatively cooled by linearly reducing the ODT depth to a final value $U_f = 0.15U_c$ (or $0.3U_c$ for the measurements on the BCS side) during various quench times t_q ranging between 0.2 s and 2.6 s (Fig. 1a). The linear relationship between the sample temperature and the ODT depth is checked by monitoring the momentum width of the thermal clouds, and a study of the condensate growth dynamics in the experiment shows that the system is well thermalized for the explored range of quench times (see Supplementary Information).

During the quench, the system undergoes a spontaneous symmetry-breaking phase transition, and superfluid domains with independent phases are formed (Fig. 1b,c). Since the ODT provides tight axial confinement, lowering the ODT depth leads to evaporation that occurs dominantly in the axial direction, along which fast thermalization is ensured. This leads to the production of domains principally in the radial plane of the sample, which merge to create vortices aligned parallel to the axial direction of the trap. To facilitate the merging dynamics, a hold time t_h of 200 ms (or 50 ms for the measurements on the BCS side) is applied after the quench, and the vortices are detected by performing time-of-flight (TOF) imaging of the sample[26]. At the end of this procedure, the sample contains about 1.0×10^6 atoms per spin state with a condensate fraction of 80% at unitarity. Representative images of the sample for a range of quench times are shown in Fig. 1d for different interaction strengths $1/k_F a$. The values of $1/k_F a$ represent the final state of the gas, where k_F is the Fermi wave number of non-interacting fermions in a harmonic trap and a is the s-wave scattering length.

Figure 2 shows the average number of observed vortices N_v as a function of t_q at four different interaction strengths across the BEC–BCS crossover. Our measurements feature an order-of-magnitude higher number of defects (up to 50 at unitarity) compared with previous KZ experiments with atomic BECs, which results from the large radial size and the short healing length of the strongly interacting Fermi superfluid. The dynamic range of the defect number spans about two orders of magnitude, and the quench duration lasts over a decade, allowing different regimes of the vortex formation dynamics to be clearly distinguished in the experiment. Specifically, for sufficiently long quench times, the evolution of the vortex number reveals the characteristic power-law scaling of the KZ mechanism, but as t_q is reduced, the vortex number becomes saturated. Such behaviour has been observed in previous KZ experiments[13,29,30], and was attributed to the presence of destructive interactions among the defects. To systematically distinguish the two regimes and reliably extract the KZ exponent, we adopt an empirical model of the defect number $N_v = N_{sat}[1 + (t_q/t_{sat})^{2\beta_{KZ}}]^{-1/2}$ proposed in ref. [29], where N_{sat} is the saturated vortex number, t_{sat} is the characteristic quench time for the onset of saturation, and β_{KZ} is the scaling exponent from this model. The model fits the data well in all of the interaction regimes,

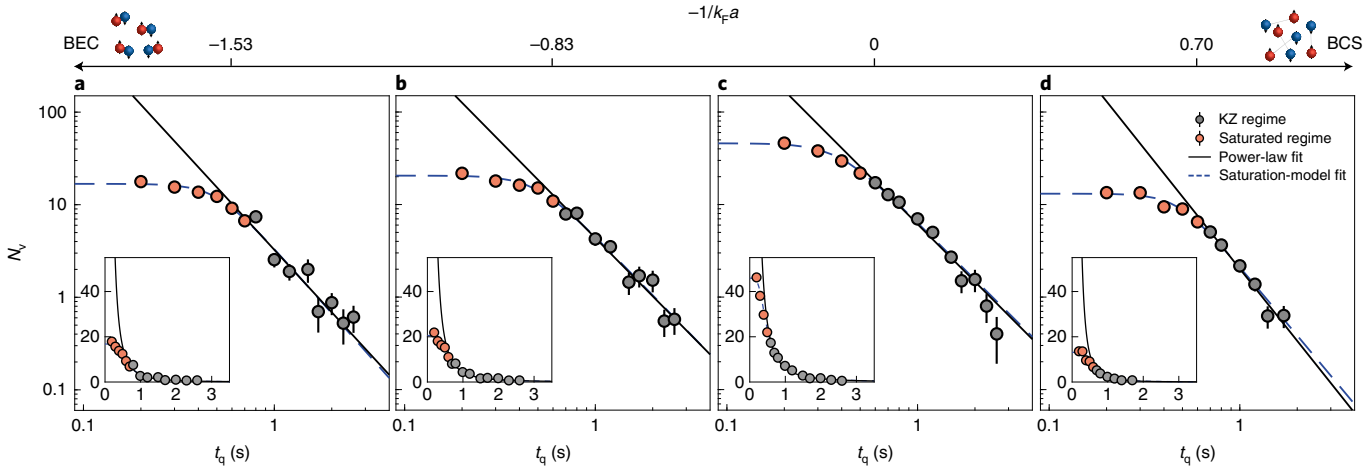

Fig. 2 | Vortex number versus quench time. The average number of detected vortices are plotted as a function of t_q on log–log axes at four different final interaction strengths $-1/k_F a = -1.53$ (757 G) (**a**), −0.83 (785 G) (**b**), 0 (832 G) (**c**) and 0.70 (898 G) (**d**). The insets show the same data on linear–linear axes. Each data point comprises at least ten realizations of the same experiment, and the error bars are the standard error of the mean. When the error bars are not visible, they are smaller than the marker size.

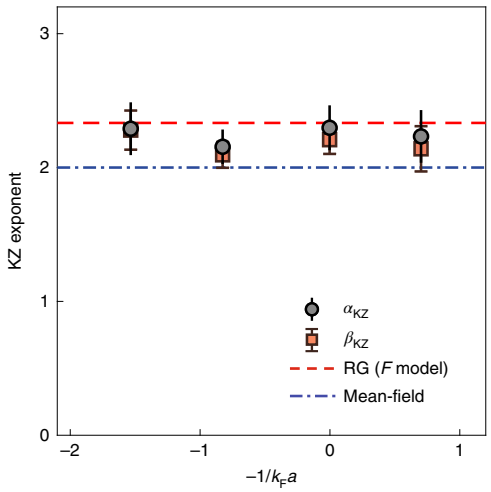

Fig. 3 | Kibble–Zurek exponents in the BEC–BCS crossover. The KZ exponents obtained from the power-law fits to the KZ regime and the model fits to the full regime are shown for the explored interaction strengths. Each data point is the average of three sets of experimental measurements, and the error bars are the quadrature sums of the standard error of the mean and the fit error. The average gives $\alpha_{KZ} = 2.24(9)$ and $\beta_{KZ} = 2.18(10)$. The predictions of the *F* model and mean-field are also shown.

suggesting the existence of a universal scaling of the vortex number even in the presence of saturation. From these fits, we identify the KZ regime through the condition $t_q \gtrsim 1.5 t_{sat}$, and a power-law function $N_v = C t_q^{-\alpha_{KZ}}$ is fit in this regime to extract the KZ exponent α_{KZ}.

A summary of the measured KZ exponents for the experimentally explored interaction strengths are shown in Fig. 3. The central observation is that, within the experimental resolution, α_{KZ} maintains a constant value across the BEC–BCS crossover, arising from the global $U(1)$ gauge symmetry of the system. The values of α_{KZ} range between 2.15 and 2.30, and their average (statistical uncertainty) yields $\alpha_{KZ} = 2.24(9)$. To put these numbers in perspective, we compare the measured values of α_{KZ} to theoretical predictions of the KZ exponent in various scenarios. For a homogeneous system, the KZ exponent is given by $(D-d)\nu/(1+\nu z)$ (ref. [2]), where D is the dimensionality of the system and d is the dimensionality of the defects. However, for an inhomogeneous sample confined in a harmonic trap, condensates with locally chosen phases are created only where the velocity of the transition front is faster than the propagation speed of the phase information. A modification of the KZ exponent to

$$(D-d)\frac{1+2\nu}{1+\nu z} \quad (1)$$

was predicted in ref. [28]. With $D-d=2$ for point defects created in an effective two-dimensional (2D) sample and the values of ν and z for the lambda transition of superfluid helium-4, the mean-field and the renormalization group theory (*F* model) predictions of the KZ exponents are 1/2 and 2/3 for a homogeneous system and 2 and 7/3 for a harmonically trapped system, respectively. The measured α_{KZ} departs far from the homogeneous case but lies between the predictions for a harmonic trap, closer to that of the *F* model. However, an improved signal-to-noise ratio is necessary to firmly distinguish between the mean-field and *F* model predictions. In light of the Ginzburg criterion, our sample is expected to be away from the mean-field regime, since the freeze-out correlation length at $-1/k_F a = -1.53$ (which is the most weakly interacting regime explored on the molecular side of the resonance) is estimated to be $\hat{\xi} \approx 10\,\mu m$ at $t_q = 200\,ms$, more than two orders of magnitude longer than the characteristic Ginzburg length $\xi_G = \lambda_{dB,c}^2/(\sqrt{128}\,\pi^2|a|) \lesssim 0.05\,\mu m$ (ref. [31]). Here, $\lambda_{dB,c}$ is the thermal de Broglie wavelength at the critical point. Note that as the interaction strength is tuned closer to resonance, the system is expected to move further away from the mean-field regime[32,33]. On the BCS side, the mean-field description should be recovered rapidly, but the data at $-1/k_F a = 0.70$, which is still within the strongly interacting regime, show no observable change in the KZ exponent.

The saturation of the vortex number at short quench times enables exploration of the microscopic aspects of defect formation dynamics near the critical point. As mentioned, the likely cause for this behaviour is the destructive interactions among vortices and antivortices, which are consistent with the observed enhancement of the vortex decay rate in the saturated regime (see Supplementary Information). Such interactions would have already taken effect during the domain merging dynamics, which is a highly entangled process of both the creation and annihilation of vortices. To estimate the saturated vortex number and understand its dependence

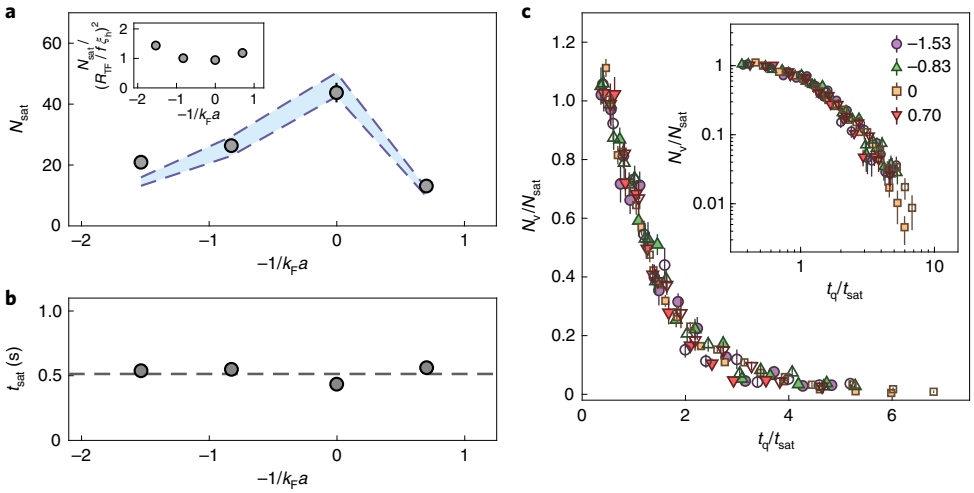

Fig. 4 | Characterization of spontaneous vortex formation across the BEC–BCS crossover. a, Comparison between N_{sat} (grey circles) and $R_{TF}^2/(f\xi_h)^2$ (blue band), including a scaling factor $f \approx 40$. The inset shows the ratio between the two values. The data points are obtained from the model fit applied to a single set of experiments, and the error bars represent the corresponding fit error. The blue band is derived from the uncertainties in R_{TF} and k_F in the experiment. **b**, Quench time t_{sat} at the onset of saturation. The error bars, which represent the corresponding fit error, are smaller than the data points. The dashed line is a guide to the eye, indicating the average of the data points. **c**, Normalized vortex number N_v/N_{sat} as a function of the normalized quench time t_q/t_{sat} at four different interaction strengths across the BEC–BCS crossover. The open markers show an independent measurement with slightly lower atom numbers. The error bars are the standard error of the mean. The inset shows the same data on log–log axes for comparison.

on $1/k_Fa$, we adopt a simple phenomenological model in which the effective range of the destructive vortex interactions during the coarsening dynamics is proportional to the vortex core size ξ_{vor}. The maximal vortex number will then be given by $(R_{TF}/f\xi_{vor})^2$, where R_{TF} is the experimentally determined Thomas–Fermi radius of the superfluid, and f is a scaling factor that accounts for the characteristic distance. Since f is a geometric factor that captures the effective size of a vortex, it is reasonable to expect that its value is fairly constant within the crossover. A mean-field estimate of N_{sat} can then be obtained by substituting ξ_{vor} with the superfluid healing length $\xi_h = \hbar/mv_c$, where m is the atomic mass of ^{6}Li and v_c is the mean-field Landau critical velocity of the superfluid sample at its centre.

Figure 4a compares the experimentally obtained values of N_{sat} with their mean-field estimates in the BEC–BCS crossover, and the inset shows their ratios. The scaling factor f has been determined to be ~40 by fitting the theory to the data using least squares. The dependence of N_{sat} on $1/k_Fa$ is captured exceptionally well by the mean-field theory, where the slight variations of the ratios in the strongly interacting regime (shown in the inset) may imply the presence of beyond-mean-field corrections to ξ_h and also possible weak variations in f. Figure 4b summarizes the corresponding quench times t_{sat} where saturation begins to develop. Note that to account for the higher final trap depth used for the data taken at $-1/k_Fa = 0.70$, the corresponding value of t_{sat} has been rescaled to match the quench rates. In contrast to N_{sat}, t_{sat} maintains a fairly constant value within the investigated interaction strengths. Since the thermalization rate of the system would not show a sharp peak at unitarity[34], a weak dependence of t_{sat} on $1/k_Fa$ is expected. However, a full understanding of this behaviour will require enhanced modelling of the quench profile at each interaction strength $1/k_Fa$ and knowledge of the interaction dependence of the microscopic parameters ξ_0 and τ_0 near the critical point. Using the N_{sat} and t_{sat} values extracted from the model fits to the data, the measured vortex numbers and their respective quench times can be rescaled to collapse the full data into a single universal curve representing the quench dynamics of vortex formation in this system throughout the different quench regimes, as shown in Fig. 4c. This provides a benchmark for theoretical studies of the quench production of defects in a strongly interacting Fermi superfluid and for its related systems such as weakly interacting BECs and superfluid helium.

An extension of this work will be to perform a similar set of measurements in the weak-fluctuation limit, where the system's freeze-out correlation length is shorter than ξ_G and the mean-field description of its critical dynamics is restored. A precise measurement of the evolution of the KZ exponent as the system is tuned further away from unitarity in the BEC regime will characterize the role of fluctuations. The use of tailored optical potentials to confine the atoms in a quasi-2D geometry offers an additional means of controlling the role of fluctuations. In 2D, the Landau–Ginzburg description of phase transitions breaks down, and superfluidity arises through the infinite-order Berezinskii–Kosterlitz–Thouless transition. Here, the exponential divergence of the correlation length and relaxation time has been predicted to give rise to a logarithmic correction to the KZ exponent[35].

Online content

Any methods, additional references, Nature Research reporting summaries, source data, statements of code and data availability and associated accession codes are available at https://doi.org/10.1038/s41567-019-0650-1.

Received: 15 March 2019; Accepted: 26 July 2019;
Published online: 16 September 2019

References

1. Kibble, T. W. Topology of cosmic domains and strings. *J. Phys. A* **9**, 1387–1398 (1976).
2. Zurek, W. H. Cosmological experiments in superfluid helium? *Nature* **317**, 505–508 (1985).
3. Sonner, J., del Campo, A. & Zurek, W. H. Universal far-from-equilibrium dynamics of a holographic superconductor. *Nat. Commun.* **6**, 8406 (2015).
4. Chesler, P. M., García-García, A. M. & Liu, H. Defect formation beyond Kibble-Zurek mechanism and holography. *Phys. Rev. X* **5**, 021015 (2015).
5. Bulgac, A., Luo, Y. L., Magierski, P., Roche, K. J. & Yu, Y. Real-time dynamics of quantized vortices in a unitary Fermi superfluid. *Science* **332**, 1288–1291 (2011).

6. Adams, A., Carr, L. D., Schäfer, T., Steinberg, P. & Thomas, J. E. Strongly correlated quantum fluids: ultracold quantum gases, quantum chromodynamic plasmas and holographic duality. *New J. Phys.* **14**, 115009 (2012).
7. Hohenberg, P. C. & Halperin, B. I. Theory of dynamic critical phenomena. *Rev. Mod. Phys.* **49**, 435–479 (1977).
8. Chuang, I., Durrer, R., Turok, N. & Yurke, B. Cosmology in the laboratory: defect dynamics in liquid crystals. *Science* **251**, 1336–1342 (1991).
9. Hendry, P. C., Lawson, N. S., Lee, R. A. M., McClintock, P. V. E. & Williams, C. D. H. Generation of defects in superfluid ^{4}He as an analogue of the formation of cosmic strings. *Nature* **368**, 315–317 (1994).
10. Bäuerle, C., Bunkov, Y. M., Fisher, S. N., Godfrin, H. & Pickett, G. R. Laboratory simulation of cosmic string formation in the early Universe using superfluid ^{3}He. *Nature* **382**, 332–334 (1996).
11. Ruutu, V. M. H. et al. Vortex formation in neutron-irradiated superfluid ^{3}He as an analogue of cosmological defect formation. *Nature* **382**, 334–336 (1996).
12. Pyka, K. et al. Topological defect formation and spontaneous symmetry breaking in ion Coulomb crystals. *Nat. Commun.* **4**, 2291 (2013).
13. Ulm, S. et al. Observation of the Kibble–Zurek scaling law for defect formation in ion crystals. *Nat. Commun.* **4**, 2290 (2013).
14. Ejtemaee, S. & Haljan, P. C. Spontaneous nucleation and dynamics of kink defects in zigzag arrays of trapped ions. *Phys. Rev. A* **87**, 051401 (2013).
15. Weiler, C. N. et al. Spontaneous vortices in the formation of Bose-Einstein condensates. *Nature* **455**, 948–951 (2008).
16. Lamporesi, G., Donadello, S., Serafini, S., Dalfovo, F. & Ferrari, G. Spontaneous creation of Kibble-Zurek solitons in a Bose-Einstein condensate. *Nat. Phys.* **9**, 656–660 (2013).
17. Corman, L. et al. Quench-induced supercurrents in an annular Bose gas. *Phys. Rev. Lett.* **113**, 135302 (2014).
18. Navon, N., Gaunt, A. L., Smith, R. P. & Hadzibabic, Z. Critical dynamics of spontaneous symmetry breaking in a homogeneous Bose gas. *Science* **347**, 167–170 (2015).
19. Giorgini, S., Pitaevskii, L. P. & Stringari, S. Theory of ultracold atomic Fermi gases. *Rev. Mod. Phys.* **80**, 1215–1274 (2008).
20. Zwerger, W. (ed.) *Lecture Notes in Physics: The BCS–BEC Crossover and the Unitary Fermi Gas* Vol. 836 (Springer, 2011).
21. Nozières, P. & Schmitt-Rink, S. Bose condensation in an attractive fermion gas: from weak to strong coupling superconductivity. *J. Low. Temp. Phys.* **59**, 195–211 (1985).
22. Regal, C. A., Greiner, M. & Jin, D. S. Observation of resonance condensation of fermionic atom pairs. *Phys. Rev. Lett.* **92**, 040403 (2004).
23. Chen, Q., Regal, C. A., Greiner, M., Jin, D. S. & Levin, K. Understanding the superfluid phase diagram in trapped Fermi gases. *Phys. Rev. A* **73**, 041601 (2006).
24. Miller, D. E. et al. Critical velocity for superfluid flow across the BEC-BCS crossover. *Phys. Rev. Lett.* **99**, 070402 (2007).
25. Weimer, W. et al. Critical velocity in the BEC-BCS crossover. *Phys. Rev. Lett.* **114**, 095301 (2015).
26. Park, J. W., Ko, B. & Shin, Y. Critical vortex shedding in a strongly interacting fermionic superfluid. *Phys. Rev. Lett.* **121**, 225301 (2018).
27. Heiselberg, H. Fermi systems with long scattering lengths. *Phys. Rev. A* **63**, 043606 (2001).
28. del Campo, A., Retzker, A. & Plenio, M. B. The inhomogeneous Kibble–Zurek mechanism: vortex nucleation during Bose–Einstein condensation. *New J. Phys.* **13**, 083022 (2011).
29. Donadello, S. et al. Creation and counting of defects in a temperature-quenched Bose-Einstein condensate. *Phys. Rev. A* **94**, 023628 (2016).
30. Liu, I. K. et al. Dynamical equilibration across a quenched phase transition in a trapped quantum gas. *Comm. Phys.* **1**, 24 (2018).
31. Donner, T. et al. Critical behavior of a trapped interacting Bose gas. *Science* **315**, 1556–1558 (2007).
32. Taylor, E. Critical behavior in trapped strongly interacting Fermi gases. *Phys. Rev. A* **80**, 023612 (2009).
33. Debelhoir, T. & Dupuis, N. Critical region of the superfluid transition in the BCS-BEC crossover. *Phys. Rev. A* **93**, 023642 (2016).
34. Gehm, M. E., Hemmer, S. L., O'Hara, K. M. & Thomas, J. E. Unitarity-limited elastic collision rate in a harmonically trapped Fermi gas. *Phys. Rev. A* **68**, 011603 (2003).
35. Jelić, A. & Cugliandolo, L. F. Quench dynamics of the 2d *XY* model. *J. Stat. Mech.* **2011**, P02032 (2011).

Acknowledgements

We thank A. del Campo for discussions. This work was supported by the Institute for Basic Science in Korea (grant no. IBS-R009-D1) and the National Research Foundation of Korea (grant no. NRF-2018R1A2B3003373). J.W.P. acknowledges support from the POSCO Science Fellowship of the POSCO TJ Park Foundation.

Author contributions

J.W.P. and Y.S. conceived the idea. B.K. and J.W.P. performed the experiment and data analysis. J.W.P. and B.K. wrote the manuscript, and all authors discussed the results and commented on the manuscript. J.W.P. and Y.S. supervised the project.

Competing interests

The authors declare no competing interests.

Additional information

Supplementary information is available for this paper at https://doi.org/10.1038/s41567-019-0650-1.

Reprints and permissions information is available at www.nature.com/reprints.

Correspondence and requests for materials should be addressed to J.W.P. or Y.S.

Peer review information: *Nature Physics* thanks Nikolaos Proukakis and the other, anonymous, reviewer(s) for their contribution to the peer review of this work.

Publisher's note: Springer Nature remains neutral with regard to jurisdictional claims in published maps and institutional affiliations.

Methods

Sample preparation. A detailed description of our experimental set-up and the preparation of a strongly interacting Fermi gas of ^{6}Li is given in ref. [26]. After standard laser cooling procedures and sympathetic cooling by bosonic ^{23}Na atoms, a balanced mixture of the two lowest hyperfine states of fermionic ^{6}Li atoms is prepared in a single-beam ODT (with an aspect ratio of 110:1) at 815 G, close to the Feshbach resonance at 832 G. The mixture is further cooled by reducing the ODT beam intensity to a value that corresponds to a trap depth of $U_i = 1.15U_c(B)$, where $U_c(B)$ is the critical ODT depth for the onset of condensation at magnetic field B. Since U_c depends on the interaction strength, its value for a given atom number is determined at each B accessed in the experiment by examining the condensate fraction as a function of the trap depth. The magnetic field is adiabatically ramped to the magnetic field B at which the thermal quench will be performed.

At this stage of the experiment before the thermal quench, the gas is composed of approximately 2.0×10^6 ^{6}Li atoms per spin state for all the explored values of B. The trapping frequencies in the radial plane of the sample are $(\omega_x, \omega_y) = 2\pi \times (20, 19)$ Hz, and the axial trapping frequency ranges between $\omega_z = 2\pi \times 1{,}080$ Hz at 757 G and 780 Hz at 898 G, depending on the explored interaction regimes. Following the quench, the final radial trap frequency is about 17 Hz, and the axial trap frequency ranges between 350 Hz and 400 Hz. Here, the radially symmetric confinement is dominantly provided by the residual magnetic curvature of the Feshbach field, and the tight axial confinement is provided by the ODT. The variation in ω_x and ω_y for the explored range of B is negligible.

Detecting vortices. The spontaneously created vortices are manifested as density-depleted holes in TOF images of the gas. The detection sequence begins by simultaneously switching off the ODT and rapidly decreasing the Feshbach field to a value close to zero. This initiates the TOF expansion of the sample and converts the fermion pairs into tightly bound molecules[22]. The sample freely expands for 13.5 ms, and the magnetic field is then quickly ramped to 695 G in 10 ms, where an absorption image of the gas is taken. Owing to the tight axial confinement provided by the ODT, the condensate rapidly expands in the axial direction on its release, and the radial size remains fairly constant during the TOF.

For the experiments performed at 898 G on the BCS side of the resonance, the vortex visibility is reduced because of the higher thermal fraction of the sample. To enhance the depletion contrast and help identify the vortices, we ramp the magnetic field from 898 G to 855 G in 5 ms before releasing the gas from the trap. This additional ramping increases the condensate fraction of the sample and boosts the contrast of the depletion[36]. We check that this procedure does not influence the number of observed vortices by comparing the number with and without the ramp.

The number of vortices in TOF images is automatically counted by an image processing method with the analysis of the hole area (see Supplementary Information).

Data availability

The data supporting this manuscript are available from the corresponding authors on reasonable request.

References

36. Zwierlein, M. W., Schirotzek, A., Schunck, C. H. & Ketterle, W. Vortices and superfluidity in a strongly interacting Fermi gas. *Nature* **435**, 1047–1051 (2005).